Journal of Nano- and Electronic Physics
Vol. **14** No 2, 02011(5pp) (2022)

Журнал нано- та електронної фізики
Том **14** № 2, 02011(5cc) (2022)

Rapid Wet Chemical Synthesis of Cuprous Oxide (Cu_2O) Nanoparticles: Effect of Precursor Concentration

Sachin S. Sawant, Chandrashekhar M. Mahajan*

Department of Engineering Sciences and Humanities, Vishwakarma Institute of Technology, Pune – 411037, Maharashtra, India

(Received 16 February 2022; revised manuscript received 18 April 2022; published online 29 April 2022)

Rapid synthesis of Cu_2O nanoparticles was carried out by wet chemical synthesis technique. The effect of $CuSO_4$ precursor molar concentration (0.05-0.15 mol) on the structural, morphological and optical properties of Cu_2O nanoparticles is reported. X-ray diffraction analysis of the synthesized Cu_2O powder shows a cubic structure with nanocrystalline nature. The average crystallite size of Cu_2O nanoparticles increases from 10 to 25 nm with increasing precursor molarity. Scanning Electron Microscopic (SEM) analysis shows nanocrystalline Cu_2O formation with increased particle size due to rise in molarity. The FTIR spectroscopic analysis ascertains the presence of characteristic functional groups in Cu_2O. UV-Vis spectra show a characteristic absorbance peak around 485 nm attributed to Cu_2O. The energy band gap measurements from the Tauc plot reveal a decrease in band gap energy with increasing precursor molarity owing to increased grain size. The band gap energy decreases from 2.94 to 2.64 eV due to an increase in the grain size mainly due to quantum confinement effect.

Keywords: Cuprous oxide, Nanoparticles, Structural properties, Optical properties, FTIR analysis.

DOI: 10.21272/jnep.14(2).02011 PACS numbers: 61.05.Cp, 61.46.Df, 68.37.Ma, 78.40.Kc

1. INTRODUCTION

In recent times, the propitious properties, ensuing potential applications in the diversified fields, have led researchers to focus on nanocrystalline semiconductor transition metal oxides, especially on cuprous oxide (Cu_2O). Being a *p*-type semiconductor with 2.2 eV as a direct band gap energy value, copious availability and nontoxic nature substantiate its great prospects and prominence for the industry.

Very recently, Cu_2O nanoparticles have shown great potential for environmental sustainability through electrochemical reduction of CO_2 [1]. They are also used in solid state lighting devices such as perovskite-based light-emitting diodes [2]. Besides these, other key areas, in which Cu_2O nanoparticles have given profound contribution, are sensors [3], lithium-ion batteries [4], solar cells [5], photocatalysis [6], printed electronics for ink preparation [7], potassium-ion batteries [8], electrocatalytic degradation [9], antibacterial application [10], and in photocatalytic degradation of 4-aminopyridine [11].

In nano regime, nanostructured materials show size dependent properties, hence it demands appropriate synthesis conditions being implemented meticulously to obtain them. A variety of wet synthesis techniques to synthesize nano Cu_2O have been explored [12]. The recent reports show nano Cu_2O synthesis on silica nanoparticle surface [13] also by using phytochemical assisted synthesis [14] and even through green synthesis route [15].

To obtain Cu_2O nanoparticles, a wet chemical synthesis route is preferred. The choice of this route is not only due to its executional simplicity but also its flexibility to effectively monitor and control its various reaction parameters, such as the precursor and its molarity, solvent, surfactant, catalyst and temperature.

Here, the crucial effect of precursor molarity (Copper Sulphate (C.S.)) on the structural, morphological, and optical properties of Cu_2O nanoparticles is reported.

2. EXPERIMENTAL

2.1 Materials

The wet chemical route for swift synthesis of Cu_2O nanoparticles requires analytical reagent grade copper sulphate pentahydrate ($CuSO_4$, $5H_2O$), sodium hydroxide (NaOH), the reducing agent L- ascorbic acid ($C_6H_8O_6$) and capping agent polyvinylpyrrolidone (PVP) (K30, Molecular weight 60,000). These chemicals were procured from Loba Chemie private limited and were used without further purification for synthesis.

2.2 Method

The wet chemical synthesis route for rapid synthesis of Cu_2O nanoparticles is as reported in our previous work [29]. The aqueous solutions of $CuSO_4$ (0.05, 0.10 and 0.15 mol), NaOH (0.2 mol), $C_6H_8O_6$ (0.1 mol) and PVP (0.6 mmol) are prepared in double distilled water. The PVP surfactant solution is added in C.S. solution, immediately trailed by the simultaneous addition of NaOH and $C_6H_8O_6$ solutions to obtain instant yellow-orange colored precipitate of Cu_2O nanoparticles. Then the precipitate is filtered and washed by double distilled water. The precipitate can be further dried in an oven at 60 °C to obtain finely powdered yellow-orange colored Cu_2O nanoparticles.

2.3 Characterization

X-ray diffraction (XRD) analysis of powder samples of nano Cu_2O was done to determine the crystal structure and average crystallite size. The XRD system

* c_mahajan9@yahoo.com

(Bruker D-8, Billerica, MA) at 40 kV and 30 mA emits CuKα radiation source of $\lambda = 1.5406$ Å. The scanning was carried out over 20-80° with a scan speed of 0.02°/s. The Field Emission Scanning Electron Microscope (FESEM) (Make – JOEL, 7000) was used to reveal the surface morphology of Cu_2O nanoparticles. Cu_2O grafted KBr powder samples were analyzed for characteristic functional group by FTIR spectrometer in the range of 4000-400 cm^{-1}. The ultrasonicated colloidal dispersions of Cu_2O nanoparticles in double distilled water were used for optical absorbance measurements by UV-Vis spectrophotometer (Shimatzu 1650PC).

3. RESULTS AND DISCUSSION

3.1 Structural Properties and Morphology

Fig. 1 depicts the XRD patterns of as synthesized Cu_2O nanoparticles for $CuSO_4$ molar concentrations of 0.05, 0.1 and 0.15 mol. The XRD patterns show nanocrystalline Cu_2O formation with characteristic peaks alike to the standard powder diffraction pattern for Cu_2O (JCPDS Card No.05 – 0667). The XRD for Cu_2O particles (0.05 mol of C.S.) shows the peak broadening, indicating the smaller crystallite size. The lower C.S. concentration during synthesis and excess control of surfactant PVP together contribute to inhibition of agglomeration and growth of Cu_2O [30]. At lower C.S. concentrations, the XRD shows minor traces of Cu and CuO nanoparticle formation ascribed to (111) peak for Cu at 43.3° and $(\bar{2}02)$ peak for CuO at 48.5°. The stoichiometric balance of the precursors is one of the criteria to get single phase Cu_2O with no traces of Cu and CuO. The XRD pattern for Cu_2O nanoparticles synthesized at C.S. concentration of 0.1 mol shows sharp intense peaks with reduced peak width. Thus, an increase in precursor concentration increases the rate of synthesis giving higher yield and crystallite size. At higher precursor concentrations, Cu_2O nanoparticles agglomerate quickly to form larger particles lessening the role of surfactant. The miniscule traces of Cu (111) peak can be seen at 2θ value of 43.3°. Whereas the XRD pattern of Cu_2O powder synthesized with $CuSO_4$ concentration of 0.15 mol depicts the most intense peaks with the smallest peak width. This is due to an increase in the rate of reaction and agglomeration at a higher precursor concentration. The role of surfactant PVP is further suppressed which results in increased average crystallite size. The XRD also shows tiny traces of CuO phase for $(\bar{2}02)$ peak at 2θ value of 48.5°. These minute traces of CuO secondary phase formation may be attributed to the insufficient oxygen for oxidation of C.S. due to its slight excess molar concentration as compared to other precursors [16, 17].

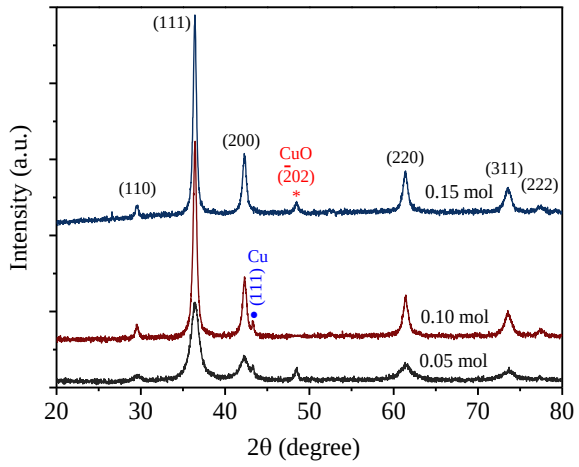

Fig. 1 – XRD patterns of Cu_2O nanoparticles prepared with varied precursor (C.S.) concentrations

The interplanar distance d was estimated by using the Bragg law from the knowledge of X-ray wavelength (λ) and Bragg angle (θ) with the first-order approximation ($n = 1$):

$$2d\sin\theta = n\lambda\,. \tag{1}$$

The average grain size D of as synthesized Cu_2O nanoparticles was calculated by Scherer formula [18]:

$$D = \frac{k\lambda}{\beta\cos\theta}\,, \tag{2}$$

where $k = 0.9$ is the shape factor and β is the full width at half maximum (FWHM). The determined average crystallite sizes were 10, 20 and 25 nm for precursor C.S. concentrations of 0.05, 0.1 and 0.15 mol, respectively. This means that with an increase in precursor concentration, there is an increase in the average crystallite size of Cu_2O nanoparticles.

The estimation of dislocation density (δ), microstrain (ε) and lattice constant (a) was done using the following relations [18]:

$$\begin{aligned}\delta &= \frac{1}{D^2}\\ \varepsilon &= \frac{\beta\cos\theta}{4}\\ a^2 &= d^2\left(h^2+hk+k^2\right)\end{aligned} \tag{3}$$

where a is the lattice constant and h, k, and l are the Miller indices. The unit cell volume (V) for cubic Cu_2O can be estimated by formula $V = a^3$.

Table 1 depicts 2θ values for (hkl) planes and interplanar distance (d), whereas Table 2 shows variation in dislocation density (δ), microstrain (ε), lattice constant (a) and cell volume (V) for Cu_2O nanoparticles synthesized at different C.S. concentrations.

SEM micrographs of Cu_2O nanoparticles samples synthesized at 0.05, 0.1 and 0.15 mol concentration of C.S. are shown in Fig. 2a, Fig. 2b, Fig. 2c, respectively. Fig. 2a displays the formation of small sized (20 nm), agglomerated Cu_2O nanoparticles. Fig. 2b depicts Cu_2O nanoparticles similar features of approximately 30 nm size. Also, Fig. 2c depicts larger cluster formation due to enhanced agglomeration effects as compared to that of Fig. 2a and Fig. 2b with particle size ranging from 30 to 60 nm. Thus, due to an increase in precursor concentration, the average particle size increases for Cu_2O nanoparticles.

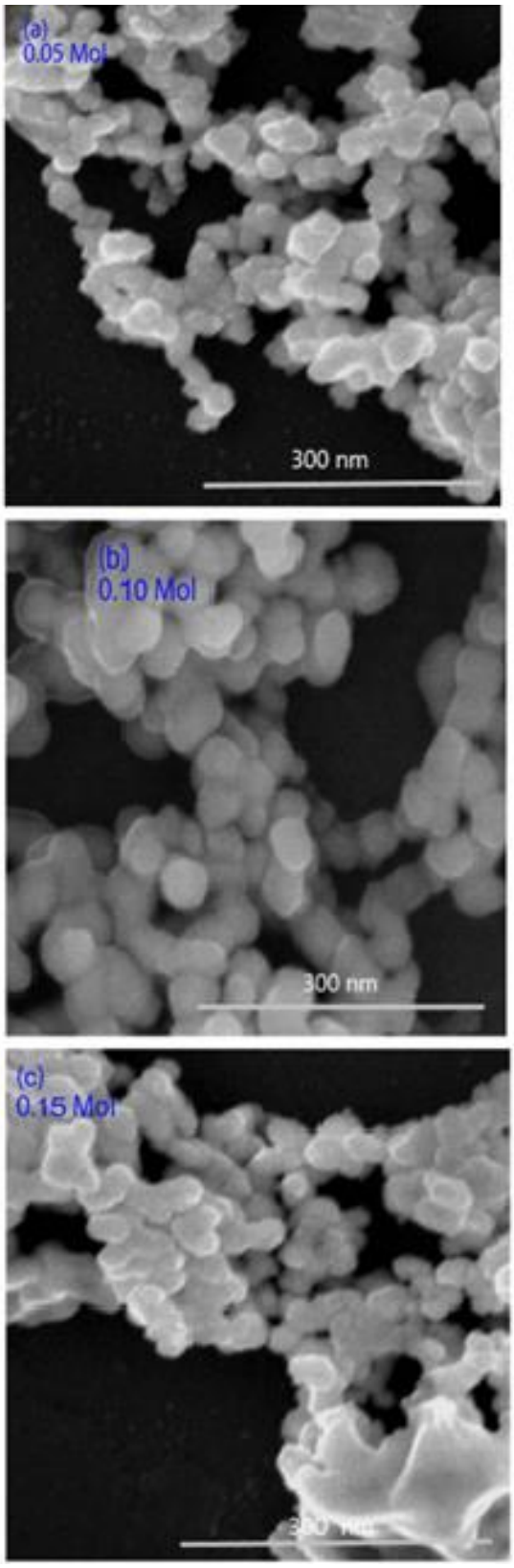

Fig. 2 – SEM micrographs of Cu_2O nanoparticles synthesized at different concentrations of C.S.: (a) 0.05, (b) 0.10, and (c) 0.15 mol

The dislocation density decreases with increasing precursor molarity mainly due to an increase in the average grain size. The values of macrostrain, lattice constant and cell volume are in good agreement with those reported in literature [18] and estimated from standard powder diffraction pattern for Cu_2O (JCPDS Card No.05 – 0667).

Table 1 – 2θ values for (hkl) planes and interplanar distances (d) from XRD for Cu_2O nanoparticles synthesized at different concentrations of C.S.

Molarity►	0.05	0.10	0.15
(hkl) plane▼	2θ		
110	29.46°	29.48°	29.46°
111	36.42°	36.40°	36.42°
200	42.30°	42.30°	42.28°
220	61.52°	61.44°	61.40°
311	73.52°	73.54°	73.58°
222	77.38°	77.42°	77.48°
(hkl) plane▼	Interplanar distance (d) in Å		
110	3.030	3.028	3.030
111	2.465	2.466	2.465
200	2.135	2.135	2.136
220	1.506	1.508	1.509
311	1.287	1.287	1.286
222	1.232	1.232	1.231

Table 2 – Variation of grain size (D), dislocation density (δ), microstrain (ε), lattice constant (a) and cell volume (V) from XRD analysis for Cu_2O nanoparticles synthesized at different C.S. concentrations

C.S. molarity	0.05	0.1	0.15
Grain size (D) nm	10	20	25
Dislocation density (δ) $\times 10^{15}$nm^{-2}	10	2.5	1.6
Microstrain (ε) $\times 10^{-2}$ line^{-2}m^{-4}	85.44	85.49	85.44
Lattice constant (a) Å	4.269	4.272	4.269
Cell volume (V) Å^3	77.82	77.95	77.82

3.2 Chemical Compositional Studies

Fig. 3 depicts the FTIR spectra of Cu_2O nanoparticles synthesized at different C.S. concentrations: 0.05, 0.1 and 0.15 mol. The wide absorption bands located at 3250.78, 3433.95 and 3439.43 cm^{-1}, respectively, for samples synthesized with increasing C.S. molarity were ascribed to H–OH stretching. Also, H–OH bending bands were observed centered at 1509.95, 1508.48 and 1510.33 cm^{-1}, respectively, for C.S. molarity variation from 0.05 to 0.15 mol. Further, for Cu_2O phase, the characteristic vibrational modes of Cu–O [16, 17] were seen at 515.95, 512.34 and 510.95 cm^{-1}, respectively, for C.S. molarity changes from 0.05 to 0.15 mol. Besides this, for 0.05 mol and 0.15 mol of C.S., Cu–O weak vibrational modes with centers at 590.23 cm^{-1} and 591.14 cm^{-1} were seen attributed to CuO phase [16, 17]. The presence of absorption bands for Cu and CuO phases in FTIR is due to stoichiometric deviation of precursors during synthesis. Table 3 shows the molecular vibrational modes as a function of wavenumber that appear in the FTIR spectra for Cu_2O nanoparticles synthesized at different C.S. concentrations.

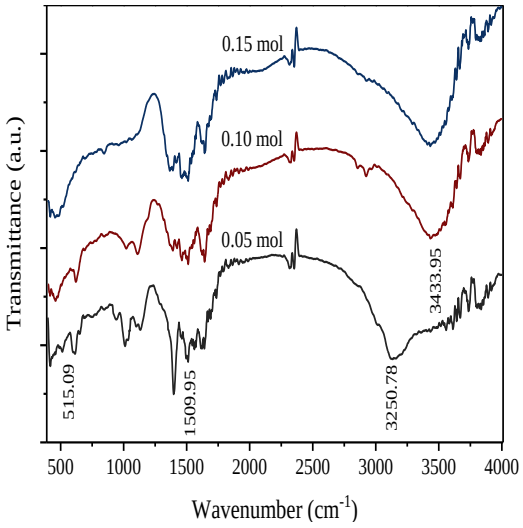

Fig. 3 – FTIR spectra of Cu_2O nanoparticles synthesized at different C.S. concentrations

Table 3 – Molecular vibrational modes and their locations centered in the FTIR spectrum for Cu_2O nanoparticles synthesized at different C.S. molarity

Molecular vibrational modes	Precursor concentration		
	0.05 mol	0.1 mol	0.15 mol
	Wavenumber (cm^{-1})		
H–OH stretching	3250.78	3433.95	3439.43
H–OH bending	1509.95	1508.48	1510.33
Cu–O vibrational	629.34	630.67	632.14
Cu–O vibrational	590.23	–	591.14
Cu–O vibrational	515.09	512.34	510.95

3.3 Optical Properties

Fig. 4 shows the measured UV-Vis spectra over the spectral range of λ of 200-800 nm for Cu_2O samples synthesized at precursor (C.S.) concentrations of 0.05, 0.1 and 0.15 mol, respectively. Fig. 4 also depicts the presence of the characteristic absorption peak around $\lambda = 463$ nm (0.05 mol), $\lambda = 474$ nm (0.1 mol), $\lambda = 487$ nm (0.15 mol) thereby affirming the formation of Cu_2O nanoparticles [19]. The peaks corresponding to Cu_2O

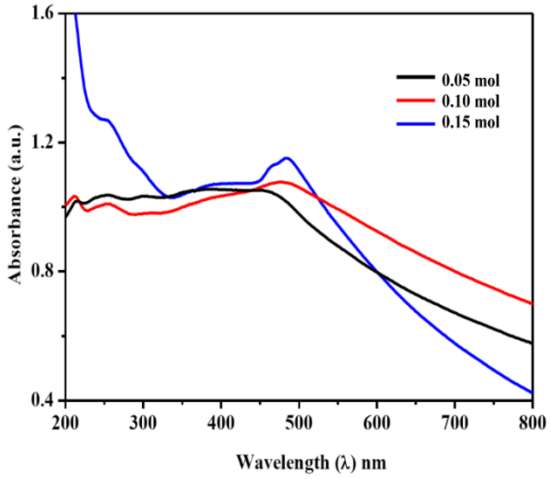

Fig. 4 – UV-Vis spectrum of Cu_2O nanoparticles synthesized at different precursor (C.S.) concentrations: 0.05, 0.1 and 0.15 mol

for these samples underwent a red shift from $\lambda = 463$ nm, 474 nm to 487 nm due to an increase in the concentration of C.S. from 0.05 to 0.15 mol. This red shift may be attributed to increased particle size due to agglomeration of Cu_2O nanoparticles at higher C.S. molarity. Interestingly, the weak secondary absorbance peaks centered at $\lambda = 280$ nm for 0.05 mol and at $\lambda = 285$ nm for 0.15 mol, respectively, were ascribed to the presence of miniscule traces of CuO [16-20]. A very weak secondary absorbance peak was observed centered at $\lambda = 348$ nm (0.05 mol), $\lambda = 350$ nm (0.1 mol) and $\lambda = 352$ nm (0.15 mol) ascribed to Cu nanoparticles [16-19]. However, the primary and characteristic peaks of Cu, generally centered in between $\lambda = 500$ to 600 nm [16-19], was not observed. Thus, UV-Vis studies again underlined that the very low presence of Cu and CuO phases observed in the samples could be attributed to different molar concentrations of the precursor C.S., thereby affecting the exact stoichiometric balance of the precursors.

The optical band gap (E_g) of Cu_2O nanoparticle samples was calculated using the Tauc relation [16-19]:

$$\alpha h\nu = \left(h\nu - E_g\right)^n, \qquad (2)$$

where α is the absorption coefficient, $h\nu$ is the photon energy and the exponent n (takes the values 1/2, 1/3, 2 and 3/2) determines the type of electronic transition that caused the absorption. By plotting $(\alpha h\nu)^{1/2}$ against $h\nu$, the best linear relationship was obtained thereby signifying the direct allowed transitions.

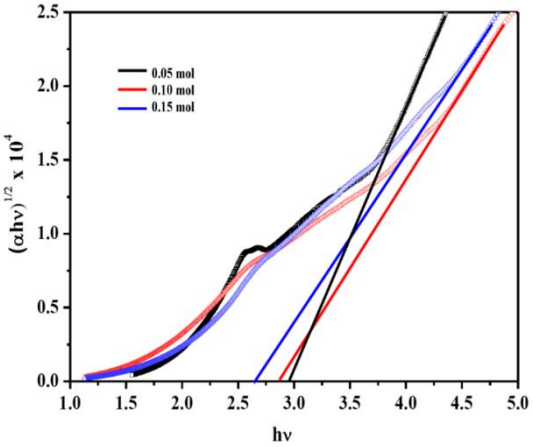

Fig. 5 – The plot of $(\alpha h\nu)^{1/2}$ vs $h\nu$ for Cu_2O nanoparticles synthesized at different precursor (C.S.) concentrations: 0.05, 0.1 and 0.15 mol

Fig. 5 represents the plot of $(\alpha h\nu)^{1/2}$ vs $h\nu$ for Cu_2O nanoparticles for the samples obtained with 0.05, 0.1 and 0.15 mol. The band gap energy E_g of these samples was found to vary from 2.92 eV, 2.8 eV to 2.64 eV due to an increase in C.S. molarity. These E_g values were higher due to quantum confinement effects arising from nanometer size as compared to $E_g = 2.2$ eV for bulk Cu_2O [8-11]. The rise in C.S. molarity causes enhanced rate of Cu_2O formation and also agglomeration leading to increased particle size and decreased energy band gap as evident from a red shift in the absorption spectra.

4. CONCLUSIONS

The effect of changing precursor molarity on the structural and optical properties of Cu_2O nanoparticles obtained by a rapid wet chemical route is investigated. The XRD analysis shows the formation of cubic nano Cu_2O with preferred orientation along $(\bar{2}02)$ plane. The minor traces of CuO and Cu nanoparticle formation are seen due to stoichiometric imbalance. The grain size for Cu_2O nanoparticles was found to increase from 10 to 25 nm due to rise in precursor concentration. The rise in C.S. molarity increases the reaction rate; and thus formed Cu_2O nanoparticles undergo agglomeration to form clusters, which leads to larger size. FTIR analysis shows all characteristic absorption bands ascribed to Cu–O vibrational mode. The UV-Vis spectra depict the presence of the characteristic absorption peak around $\lambda = 463$ nm (0.05 mol), $\lambda = 474$ nm (0.1 mol), $\lambda = 487$ nm (0.15 mol) ascribed to Cu_2O nanoparticles. The band gap energy E_g varies from 2.92 eV, 2.8 eV to 2.64 eV due to an increase in C.S. molarity.

ACKNOWLEDGEMENTS

The authors wish to thank for the support extended by the Management, Director, Vishwakarma Institute of Technology, Pune, Maharashtra, India.

REFERENCES

1. N. Hussain, M. Abdelkareem, H. Alawadhi, A. Alami, K. Elsaid, *Appl. Phys. A* **128**, 131 (2022).
2. R. Chakraborty, H. Bhunia, S. Chatterjee, A. Pal, *J. Solid State Chem.* **281**, 121021 (2020).
3. S. Singh, U. Kumar. B. Yadav, K. Kumar, R. Kant, Tripathi, K. Singh, *Res. Phys.* **15**, 102772 (2019).
4. Y. Wang, L. Cao, J. Li, L. Kou, J. Huang, Y. Feng, S. Chen, *Chem. Eng.* **391**, 123597 (2020).
5. T. Miyata, H. Tokunaga, K. Watanabe, N. Ikenaga, T. Minami, *Thin Solid Films* **697**, 137825 (2020).
6. V. Spiridonov, X.Y. Liu, S. Zezin, I. Panova, A. Sybachin, A. Yaroslavov, *J. Organomet. Chem.* **914**, 121180 (2020).
7. M. Mallik, S. Moniaa, M. Gupta, A. Ghosh, M. Toppoa, H. Roy, *J. Alloy. Compd.* **829**, 154623 (2020).
8. Ji Ma, C. Liu, *J. Colloid Interface Sci.* **594**, 352 (2021).
9. S. Mao, X. Sun, H. Qi, Z. Sun, *Sci. Total Environ.* **793**, 148492 (2021).
10. A. Zheng, S. Sabidi, T. Ohno, T. Maeda, Y. Andou, *Chemosphere* **286** Part 2, 131731 (2022).
11. P. Attri, S. Garg, J.K. Ratan, *Nanotechnol. Environ. Eng.* (2022).
12. S.S. Sawant, A.D. Bhagwat, C.M. Mahajan, *J. Nano- Electron. Phys.* **8** No 1, 01035 (2016).
13. J. Prajapati, D. Das, S. Katlakunta, N. Maramu, V. Ranjan, S. Mallick, *Inorganica Chim. Acta* **515**, 120069 (2021).
14. M. Mannarmannan, K. Biswas, *Chem. Select* **6** No 14, 3534 (2021).
15. K. Chinnaiah, V. Maik, K. Kannan, V. Potemkin, M. Grishina, M. Gohulkumar, R. Tiwari, K. Gurushankar, *J. Fluoresc.* (2022).
16. Y. Bai, T. Yang, Q. Gu, G. Cheng, R. Zheng, *Powder Technol.* **227**, 35 (2012).
17. S.S. Sawant, A.D. Bhagwat, C.M. Mahajan, *J. Nano-Electron. Phys.* **8** No 1, 01036 (2016).
18. R.D. Prabu, S. Valanarasu, V. Ganesh, M. Shkir, S. Al Faify, A. Kathalingam, *Surf. Interface Anal.* **50**, 346 (2018).
19. L. Gau, C. Murphy, *J. Mater. Chem.* **14** No 7, 735 (2004).
20. A. Mahmoud, K. Al-Qahtani, S. Alfaij, S. Al-Qahtani, F. Alsamhan, *Sci. Rep.* **11**, 12547 (2021).

Швидкий вологий хімічний синтез наночастинок оксиду міді (Cu_2O): вплив концентрації прекурсора

Sachin S. Sawant, Chandrashekhar M. Mahajan

Department of Engineering Sciences and Humanities, Vishwakarma Institute of Technology, Pune – 411037, Maharashtra, India

Швидкий синтез наночастинок Cu_2O проводили методом вологого хімічного синтезу. В роботі йдеться про вплив молярної концентрації прекурсора $CuSO_4$ (0,05-0,15 моль) на структурні, морфологічні та оптичні властивості наночастинок Cu_2O. Рентгенодифракційний аналіз синтезованого порошку Cu_2O демонструє кубічну структуру з нанокристалічною природою. Середній розмір кристалітів наночастинок Cu_2O збільшується від 10 до 25 нм із збільшенням молярності прекурсора. Аналіз скануючою електронною мікроскопією (SEM) показує утворення нанокристалічного Cu_2O зі збільшеним розміром частинок через збільшення молярності. FTIR спектроскопічний аналіз встановлює наявність характерних функціональних груп у Cu_2O. Спектри UV-Vis показують характерний пік поглинання близько 485 нм, який відноситься до Cu_2O. Вимірювання енергетичної ширини забороненої зони з графіка Тауца виявляють її зменшення зі збільшенням молярності прекурсора внаслідок збільшення розміру зерна. Енергетична ширина забороненої зони зменшується з 2,94 до 2,64 еВ за рахунок збільшення розміру зерна в основному через квантового розмірний ефект.

Ключові слова: Оксид міді, Наночастинки, Структурні властивості, Оптичні властивості, FTIR аналіз.